Phase Behavior of Mixtures of Block Copolymer and Homopolymers in Thin Films and Bulk

Unyong Jeong, Du Yeol Ryu, Dong Han Kho, Dong Hyun Lee, and Jin Kon Kim*

Department of Chemical Engineering and Polymer Research Institute, Electronic and Computer Engineering Divisions, Pohang University of Science and Technology, Kyungbuk 790-784, Korea

Thomas P. Russell*

Polymer Science and Engineering Department, University of Massachusetts at Amherst, Amherst, Massachusetts 01003

Received February 11, 2003; Revised Manuscript Received March 26, 2003

ABSTRACT: Mixtures of polystyrene-*block*-poly(methyl methacrylate) (PS−PMMA) having PMMA cylindrical microdomains with homopolymers of PMMA and poly(ethylene oxide) (PEO) were used to study the effect of the interaction between homopolymers confined to the cylindrical microdomains and the PS matrix on the microdomain spacing of the mixtures. The microdomains in all thin films are oriented perpendicular to the film surface. It was found that the miscibility between PMMA homopolymer and PMMA block in thin film was enhanced compared with that in bulk at a given molecular weight of PMMA homopolymer. Also, the PMMA homopolymer chains in thin films were more localized to the center of PMMA microdomains than in the bulk, which results in a larger increase of the lattice spacing (D) in the former. D increased rapidly at low volume fractions of PMMA homopolymer, but it approached a saturated value as the content of PMMA increased. The increase of D with increasing molecular weight of PMMA homopolymer was saturated at a certain molecular weight. For mixtures of PS−PMMA with PEO, changes in D were similar to those seen with PMMA, except that the saturation of D was reached at a much lower molecular weight compared with PMMA. This is attributed to the strong repulsion between PEO and PS that forces a stronger localization of PEO chains to the center of the PMMA microdomains. The degree of localization of the homopolymer inside the cylindrical microdomains for all mixtures is discussed in term of increase of D.

I. Introduction

Block copolymers self-assemble into periodic morphologies with well-defined size and spacing on the tens of nanometer length scale and have been extensively studied due to their potential use as functional nanostructures.[1−6] The characteristic dimensions of the morphologies are dictated by molecular weight of the copolymer, the volume fraction of the components, the Flory−Huggins segmental interaction parameter (χ) between the blocks, and the molecular architecture of the block copolymers.[7,8]

The phase behavior of a binary blend consisting of a block copolymer and a homopolymer is primarily governed by the ratio of the number of segments of the homopolymer (N_{AH}) to that (N_{AC}) of the copolymer block miscible with the homopolymer.[9−29] According to experiments,[9−13] three regimes exist depending on N_{AH}/N_{AC}: (i) wet brush (uniform distribution of the homopolymer) for $N_{AH}/N_{AC} < 1$; (ii) dry brush (localization of the homopolymer) for $N_{AH}/N_{AC} \sim 1$; and (ii) macrophase separation for $N_{AH}/N_{AC} \gg 1$. These results imply that as the weight fraction of a homopolymer having high molecular weight increases, the homopolymer is first confined (or localized) within the microdomains, and then macrophase separation occurs at higher weight fractions. The phase behavior of mixtures consisting of an AB diblock and a homopolymer C has also been investigated, and for $\chi_{AC} < 0$ enhanced miscibility is seen when compared to mixtures of AB/A (or AB/B).[14]

* To whom correspondence should be addressed: e-mail jkkim@postech.ac.kr or russell@mail.pse.umass.edu.

The dependence of lattice spacing (D) or microdomain size on molecular weight and volume fraction of added homopolymer has been studied.[9,10,13−19] In general, D increases with increasing amount of the homopolymer though the increase strongly depends on homopolymer-chain distribution within the microdomains. If the added homopolymer is localized to the center of the microdomains, D increases due to chain extension normal to the interface, whereas D does not change significantly when the homopolymer chains are uniformly mixed within the microdomains.

Only a few groups,[30−34] however, have studied the behavior of mixtures in thin film. Using neutron reflectivity on mixture of symmetric PS−PMMA and homopolymers PMMA and (or) PS in thin films, Mayes et al.[30] showed that the homopolymer is more confined (localized) to the center of lamellar microdomains with increasing molecular weight of the homopolymer. These results are in good agreement with bulk experiments[9,10,13] and subsequent thin film experiments.[33] However, there have been no reports on the behavior of thin films consisting of mixtures of an asymmetric block copolymer with a homopolymer. Here, results on such thin film mixtures on a neutral substrate and on the bulk are presented. The effect of molecular weight and the amount of the homopolymer and χ between a homopolymer and each block on the homopolymer distribution within the microdomains was studied. Each is shown to significantly influence the morphology in the thin films which lead to simple routes to control size of the nanoscopic domains in a robust manner.

10.1021/ma034179k CCC: $25.00
Published on Web 04/24/2003

Table 1. Molecular Characteristics of PMMA and PEO Homopolymers

symbols	M_w	M_w/M_n	source
SM-88	87 800	1.04	synthesized anonically in this lab
PMMA-4	4 000	1.10	Polymer Lab
PMMA-12	12 400	1.05	synthesized anonically in this lab
PMMA-30	29 700	1.06	Polymer Lab
PMMA-60	59 600	1.07	Polymer Lab
PMMA-127	127 000	1.08	Polymer Lab
PEO-0.6	640	1.21	Fluka Chem. Co.
PEO-1.5	1 500	1.18	Fluka Chem. Co.
PEO-6	6 000	1.12	Fluka Chem. Co.
PEO-18	17 500	1.10	Fluka Chem. Co.
PEO-35	35 000	1.08	Fluka Chem. Co.
PEO-56	56 300	1.05	Polymer Lab
PEO-105	105 000	1.06	Polymer Lab

II. Experimental Section

An asymmetric PS−PMMA (SM-88), having a PMMA volume fraction of 0.3 and a weight-average molecular weight (M_w) of 87 800 with a polydispersity index (PDI) of 1.03, was anionically synthesized. Homopolymers of PMMA and PEO with narrow PDI were purchased or anionically synthesized. All the polymers were used without further purification. The M_w and PDI of PMMA and PEO homopolymers are given in Table 1.

For thin film experiments, a hydroxy-terminated PS-*ran*-PMMA copolymer, having a styrene weight fraction of 0.58 and M_w of 11 000 with a PDI of 1.13, was used to produce a substrate with balanced interfacial interaction.[35] Spin-coated random copolymer films were annealed at 170 °C for 3 days under vacuum to attach the copolymers to the native SiOx layer on a silicon wafer. After rinsing with toluene, a ~6 nm thick brush of the random copolymer remained on the substrate. Thin films (31−34 nm) of mixtures of PS−PMMA and PMMA homopolymer with various volume fractions of homopolymer, ϕ_H, were prepared by spin-coating toluene solutions onto the substrate with anchored random copolymer brush. Here, ϕ_H is defined by the volume fraction of the homopolymer in total volume of the homopolymer plus the PMMA block in PS−PMMA.

For preparing thin films of mixtures of PS−PMMA and PEO homopolymer, a mixed solvent of benzene/toluene (20/80 vol/vol) was used, and the solution was spun-coat onto the neutral brush coated surface. It is noted that toluene does not dissolve PEO completely. Thin films of mixtures of PS−PMMA and homopolymers (PMMA or PEO) were annealed at 170 °C under vacuum for 2 days and then quenched to room temperature.

Film thickness was measured with a Rudolph Research AutoEL-II ellipsometer using a helium−neon laser ($\lambda = 632.8$ nm) at a 70° incidence angle. For selective removal of entire cylindrical microdomains containing the homopolymer and PMMA block, deep UV irradiation followed by acetic acid rinsing was used. Morphologies of thin films were assessed by atomic force microscope (a Digital Instruments Dimension 3000) with the tapping mode in both height and phase contrast modes.

For the preparation of bulk samples for small-angle X-ray scattering (SAXS) experiments, mixtures of PS−PMMA and PMMA homopolymer were dissolved in THF and solution-cast at room temperature. Mixtures of PS−PMMA and PEO homopolymer were dissolved in chloroform and solution-cast at room temperature for 48 h. Residual solvents in both mixtures were completely removed at 110 °C for over 24 h under vacuum. To achieve an equilibrium microdomains, the samples were annealed at 170 °C for 48 h under vacuum.

The lattice spacing of cylindrical microdomains (D) in bulk samples was measured by small-angle X-ray scattering (SAXS) on the 4C1 beamline at the Pohang Light Source (PLS), Korea, where a W/B_4C double multilayer monochromator delivered monochromatic X-rays with a wavelength (λ) of 0.1608 nm and a resolution $\Delta\lambda/\lambda \cong 0.01$ onto the sample.[36] A flat Au mirror was used to reject the higher harmonics from the beam. A 2-D CCD camera (Princeton Instruments Inc., SCX-TE/CCD-1242) was used to collect the scattered X-rays. The sample thickness was 1.5 mm, and the exposure time was 5 min.

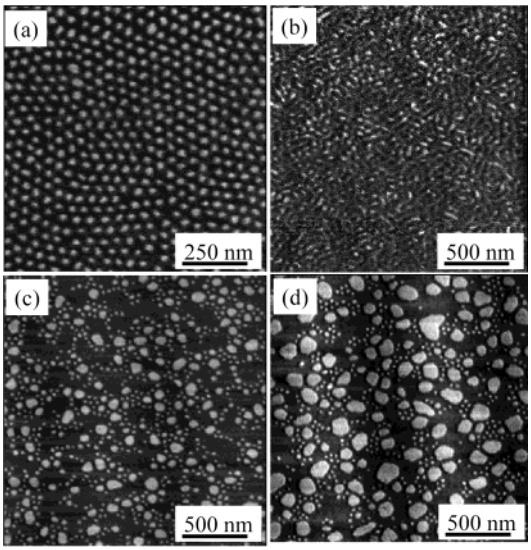

Figure 1. AFM phase images for thin films of mixtures of PS−PMMA and PMMA-60 with various volume fractions (ϕ_H): (a) 0.18, (b) 0.33, (c) 0.55, (d) 0.67. (a) and (b) show microphase separation only, whereas (c) and (d) exhibit clearly macrophase separation of PMMA homopolymer.

The lattice spacing of neat block copolymer thin film was measured by using grazing angle X-ray scattering (GAXS) on the same beamline. The incident angle of the beam varied from 0.2° to 0.6°, which is sufficient to penetrate the sample fully.

The relative lattice spacing of cylindrical microdomains (D/D_0) was obtained by Fourier transformation (FT) of scanning electron microscopy images (FE-SEM, Hitach S-4200) using the software (Scion image). SEM images were taken at 40 000× magnification after UV etching and Pt sputtering. The Fourier transformed data were circular averaged, and the position (q_{max}) of the first-order peak was obtained by the Gaussian curve fitting. Then, D was simply given by $2\pi/q_{max}$.

III. Results

Figure 1 shows the AFM phase images of thin films of mixtures of PS−PMMA with various volume fractions (ϕ_H) (0.18−0.67) of PMMA-60. Since PMMA has a higher modulus than PS chain room temperature, PMMA is brighter in AFM phase contrast images.[37,38] At lower ϕ_H (<0.2), a perpendicular orientation of the cylindrical microdomains is seen. However, as ϕ_H increases to 0.34, the cylindrical microdomains are seen to orient parallel to the substrate, even though macrophase separation is not observed. For higher ϕ_H (>0.55), macrophase separation is evident with the size of the domains increasing with increasing ϕ_H.

The AFM images given in Figure 1 represent only the surfaces of the films and provide no information on the internal morphology. Consequently, the films were exposed to UV and washed with acetic acid to remove all the PMMA chains. Figure 2a shows AFM height image of a mixture with $\phi_H = 0.55$ after removal of all the PMMA. A dark horizontal line in Figure 2a is shown, along which the height profiles are given in Figure 2b. In Figure 2b, three different height levels are seen (A > B and C > D). Microphase-separated PMMA domains with vertical orientation are observed in region A. Since the hole size of region A (~20 nm) is so small, the AFM tip does not reach the bottom of the pores, even though they span the entire thickness of the

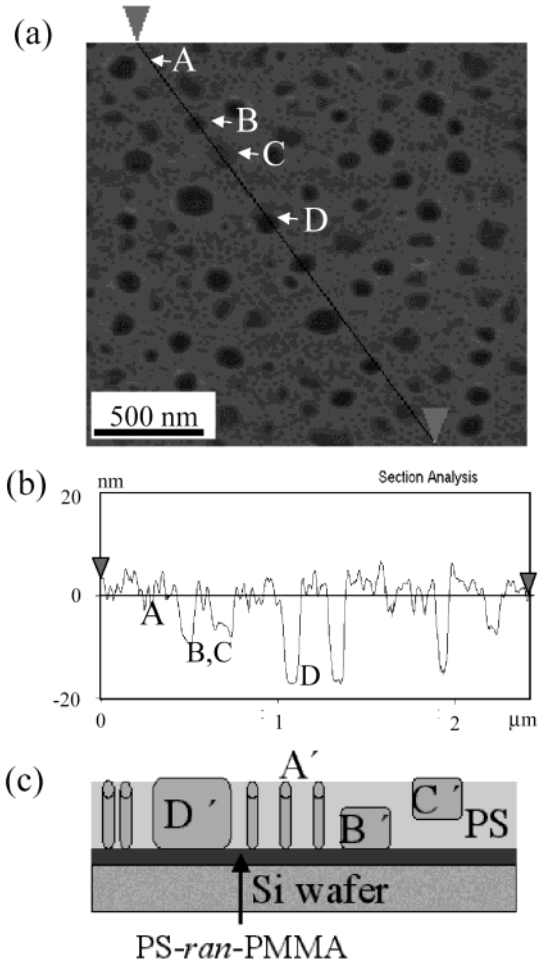

Figure 2. (a) AFM height image of the mixture of PS−PMMA and PMMA-60 with $\phi_H = 0.55$ after deep UV etching and acetic acid washing. (b) Height profiles of AFM image along the line given in AFM image. (c) A schematic showing microphase and macrophase separations. Homopolymers at region D′ touched the bottom of the film. In region B′ or C′, the homopolymer touches either the substrate or air surface. HEX microdomains with vertical orientation are clearly seen in region A′.

film, as shown previously.[4] Large empty holes in region D touching the bottom of the film are seen and indicate macrophase separation. The domain sizes in regions B and C are smaller than those in region D, but much larger than cylindrical micrdomains of PS−PMMA copolymer itself. On the basis of these results, a schematic diagram of thin films of mixtures, shown in Figure 2c, can be made. In regions with a small amount of ϕ_H, only microphase separation exists, as seen in region A′. As the volume fraction (or molecular weight) of the homopolymer increases, homopolymer chains start to segregate from copolymer microdomains as shown in regions B′ or C′, resulting in macrophase separation. We assumed that large defects without vertical orientation are found at those points. Although the AFM height images in B′ cannot be distinguished from those in C′, the size of the domains in both regions is ∼100 nm, and thus, the macrophase separation has occurred. In region D′, a coarse macrophase separation has occurred with the domains spanning the entire film thickness.

Macrophase separation in bulk samples can easily be detected by the naked eye from the turbidity. Figure 3 gives the limit of solubility of PMMA homopolymer in the mixtures for bulk samples (●) and thin films (○).

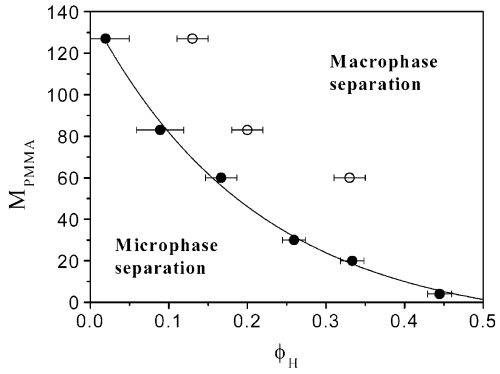

Figure 3. Solubility limits of PMMA homopolymer, above which a macrophase separation occurs, for bulk samples and thin films with various molecular weights of PMMA homopolymer. The filled circles are turbidity points in bulk samples and the solid line is a curve fitting. The open circles correspond to macrophase separation in thin film, where region B′ or C′ in Figure 2 appeared.

As mentioned above, the transition from microphase to macrophase separation is not sharp. In this study, the critical volume fraction above which macrophase separation occurs is taken as a volume fraction when the defects like B′ or C′ in Figure 2c in a mixture appear. These defects are several times the lattice spacing of the hexagonal-packed cylindrical microdomains. The error bars in Figure 3 come from the mixture composition not from the AFM image. Namely, we prepared mixtures by varying volume fractions of the homopolymer with a step of 2−3% to obtain the critical volume fraction corresponding to the macrophase separation.

The solid line is a curve to simply guide the eye. It should be noticed that, by SAXS and SEM experiments, no evidence of a change in the microdomains from cylinders to lamellae was observed for all ϕ_H employed in this study. In Figure 3, it is seen that the solubility of PMMA homopolymer in the mixtures decreases sharply with increasing molecular weight of PMMA homopolymer, in keeping with theoretical prediction.[27,28] It is also evident that the solubility of PMMA homopolymer in the thin films was greater than that in the bulk sample at a given molecular weight.

Figure 4 shows SAXS profiles (the intensity ($I(q)$) vs q ($= (4\pi/\lambda) \sin\theta$, in which λ is the wavelength and 2θ is the scattering angle in the range of $0.08 \le q \le 0.6$ nm^{-1}) as a function of ϕ_H for bulk samples with four different molecular weights of PMMA homopolymers. The SAXS profiles were shifted vertically to avoid overlap. It is found that a hexagonally packed array (HEX) of cylindrical microdomains was seen for all mixtures, evidenced by the higher order reflections at $\sqrt{3}q_{max}$ and $\sqrt{7}q_{max}$ (indicated by arrows in the figures). Here, q_{max} is the wave vector at the maximum intensity of SAXS profiles. The positions of higher order reflections were obtained through Gaussian curve fitting. From Figure 4, for a mixture with PMMA-4, q_{max} changed little even when ϕ_H was increased up to 0.45. But for mixtures with PMMA-30 and PMMA-60, q_{max} gradually shifted to lower q with increasing ϕ_H, implying that the cylinder lattice spacing (D) increased. Here, D is simply given by $2\pi/q_{max}$ and related to the interdomain distance (D_{cyl}) between two neighboring cylinders ($D_{cyl} = \sqrt{4/3}D$). For mixture with PMMA-127, q_{max} shifted very little, since macrophase separation took place at very low volume fraction ($\phi_H \sim 0.02$) of PMMA-127, as shown in Figure 3.

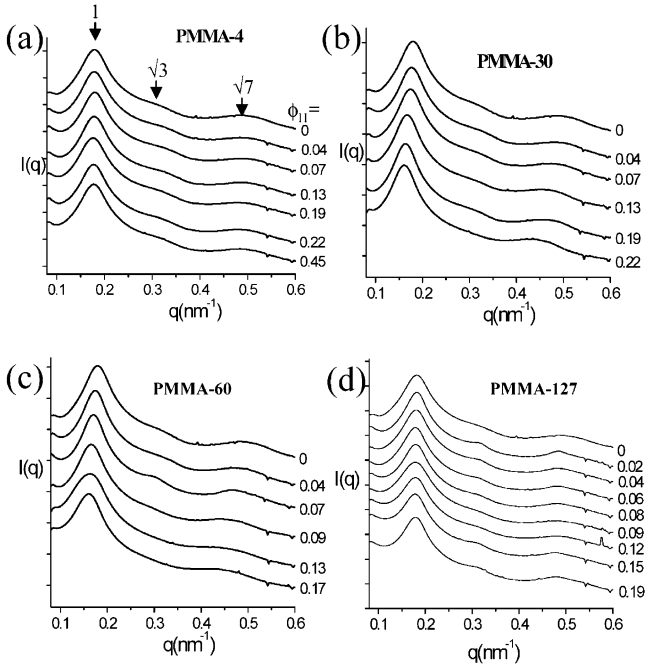

Figure 4. SAXS profiles as a function of ϕ_H for bulk mixtures with four different molecular weights of PMMA homopolymer: (a) PMMA-4, (b) PMMA-30, (c) PMMA-60, (d) PMMA-127.

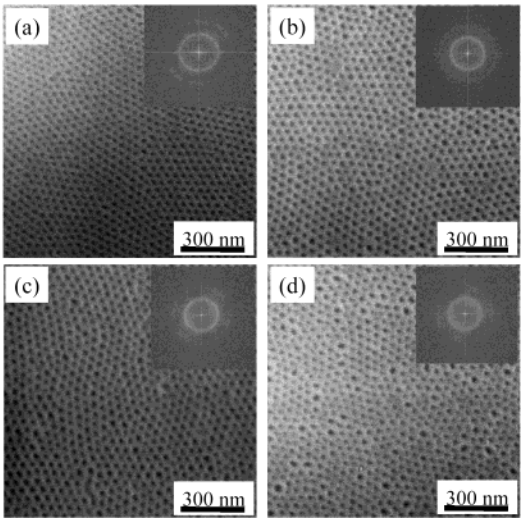

Figure 5. FE-SEM images after UV etching followed by acetic acid washing for mixtures with PMMA-127 at various values of ϕ_H: (a) 0.0, (b) 0.03, (c) 0.09, and (d) 0.13. The insets are Fourier transformation of the FE-SEM images, from which D was calculated.

Figure 5 shows SEM images for thin films of mixtures with PMMA-127 at four different ϕ_H. The Fourier transform of each SEM image was given in the inset of Figure 5. For all mixtures with $\phi_H < 0.13$, HEX cylinders oriented perpendicular to the substrate are seen. This suggests that all homopolymers are located within the PMMA microdomains of the PS−PMMA copolymer.

The lattice spacing (D_0) in bulk was obtained by SAXS; thus, the error was less than 0.1 nm. To obtain D in the thin films accurately, grazing angle X-ray scattering (GAXS) at the 4C1 beamline was used. The block copolymer film was first annealed at 170 °C for 2 days under vacuum (the same condition for the bulk sample). To enhance the contrast, PMMA cylindrical

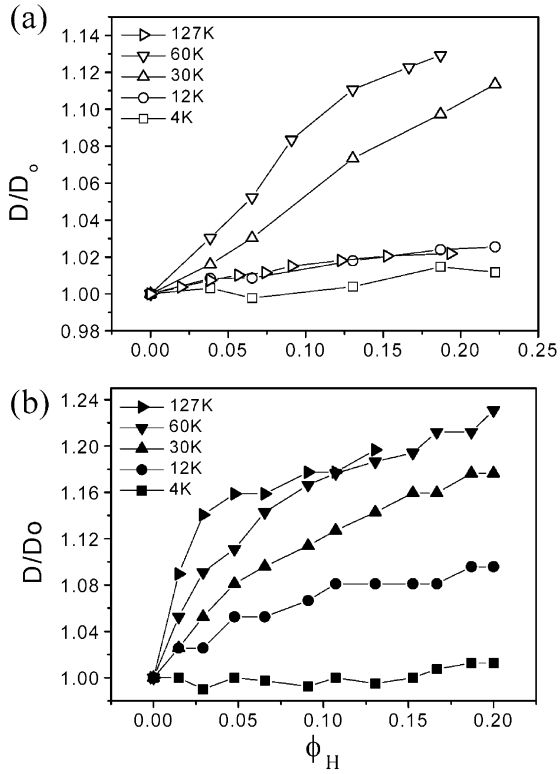

Figure 6. Increase of D with ϕ_H as a function of molecular weight of PMMA homopolymer in bulk samples (a) and thin films (b). D increase in thin films was much larger than that in bulk samples.

domains were degraded by UV and washed out by acetic acid. As shown previously,[4] this procedure does not change D_0. However, the contrast is enhanced greatly than a factor of 20. D for the thin film was found to be 35.5 ± 0.1 nm. Consequently, there is a difference (1.4 ± 0.1 nm), although not large, in D_0 between thin films and bulk sample for neat PS−PMMA, indicating that the chains in the thin film are more stretched than in the bulk due to a lateral confinement of the film by the substrate.

In Figure 6, the relative change in D, which is inversely proportional to q^*, is plotted as a function of ϕ_H for bulk samples and thin films with various molecular weights of PMMA homopolymers. D/D_0 for bulk samples given in Figure 6 were obtained from the first-order peak in the SAXS as shown in Figure 4 with the relationship of $D = 2\pi/q_{max}$. Thus, the error in determining D is less than 0.1 nm. However, D/D_0 for thin films given in Figure 6 were obtained by Fourier transformation (FT) of the SEM images as shown in the insets of Figure 5. Once FT was obtained, we can determine q_{max} corresponding to the maximum intensity peak (or first-order peak). It should be noted that the first peak in the FT's was not as sharp as that obtained by GAXS for thin films and also by SAXS for bulk samples. Furthermore, higher order peaks are hardly discernible. Yet, the maximum error in determining D was less than 0.3 nm.

For low molecular weights of PMMA (PMMA-4), D/D_0 in both thin films and bulk samples does not vary with ϕ_H. But with increasing molecular weight, D in bulk samples increases almost linearly with ϕ_H. Notice that, for the mixtures with PMMA-127 in bulk samples, D_0 did not increase much in comparison to mixtures with PMMA-60, even though the molecular weight is larger.

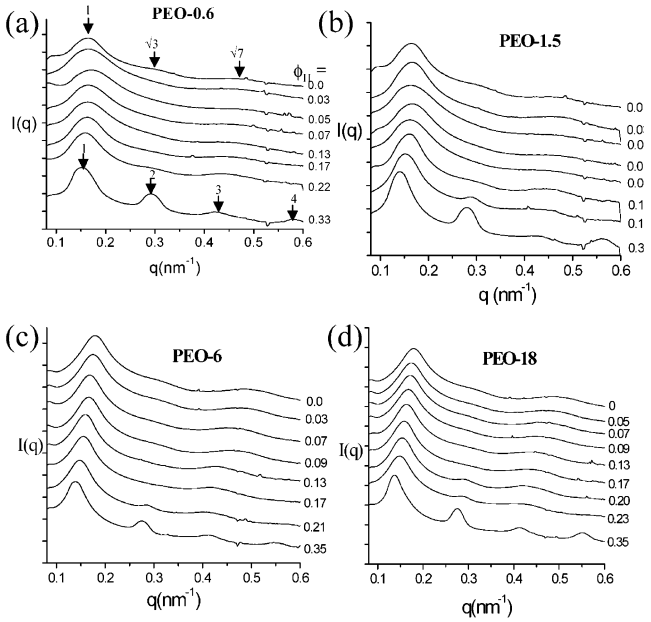

Figure 7. SAXS profiles as a function of ϕ_H for bulk mixtures with four different molecular weights of PEO homopolymer: (a) PEO-0.6, (b) PEO-1.5, (c) PEO-6, (d) PEO-18. The shift of the first-order peak position at a fixed ϕ_H became larger as the molecular weight of PMMA increased. For $\phi_H > 0.3$, higher order reflection peaks corresponding to lamellar microdomains appeared.

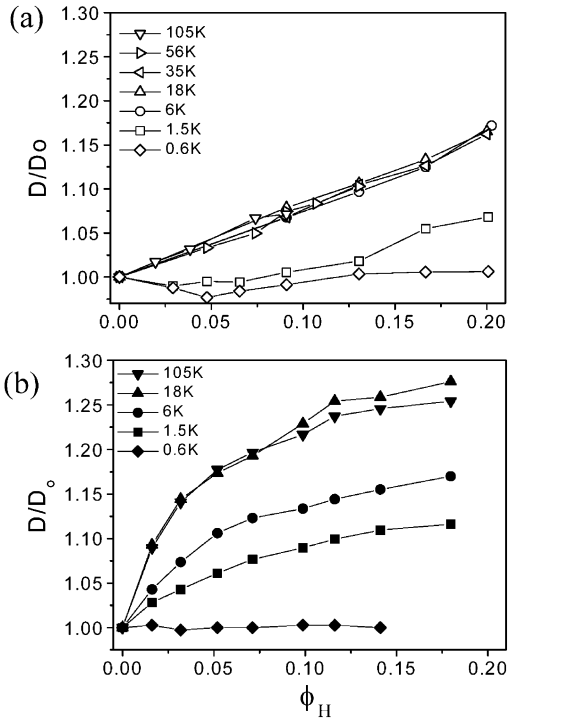

Figure 8. Increase of D with ϕ_H as a function of molecular weight of PEO homopolymer in bulk samples (a) and thin films (b).

This is because the critical volume fraction of PMMA-60, above which the macrophase separation occurs, was very low (0.02) as shown in Figure 3. For thin films, the increases in D/D_0 with ϕ_H started at lower molecular weights compared with bulk samples. For instance, D/D_0 of thin films with PMMA-12 increases gradually with ϕ_H, whereas in the bulk no increase is seen. This indicates that the degree of the localization of the homopolymer chains within the cylindrical microdomains in the thin film case is larger than that in bulk samples at a given homopolymer molecular weight. At higher molecular weights (PMMA-60, PMMA-127), D/D_0 for thin film does not change with homopolymer molecular weight. This indicates that once the homopolymer molecular weight is greater than a certain value, the degree of the localization saturates.

It is known that the degree of the localization of a homopolymer within the cylindrical microdomains depends on χ between the homopolymer and the block chains, in addition to the molecular weight and volume fraction of the homopolymer. To examine the dependence of homopolymer distribution on χ, poly(ethylene oxide) (PEO) was used. PEO has a specific dipole−dipole attraction with PMMA, whereas there is a very large repulsion with PS. χ between PS and PEO at 170 °C is 0.050 obtained from the expression of $\chi_{dPS-PEO} = -0.0067 + 25.26/T$,[39] whereas $\chi_{dPS-PMMA}$ at 170 °C is 0.028.[40]

Figure 7 shows the SAXS profiles ($0.08 \leq q \leq 0.6$ nm^{-1}) as a function ϕ_H for bulk samples of the mixtures with four different molecular weights (600−18 000) of PEO homopolymer. No macrophase separation was seen for the mixtures when $\phi_H < 0.4$. However, when $\phi_H \geq 0.20$, the cylindrical microdomains changed to lamellar microdomains, since a high-order peak at $2q_{max}$ ($3q_{max}$ and $4q_{max}$ in some mixtures) was clearly observed. Furthermore, a melting peak of the PEO homopolymer within the lamellar morphologies was found by differential scanning calorimetry. In contrast, for the mixtures with PMMA homopolymer, this morphological transformation was not observed, even for $\phi_H > 0.2$.

Figure 8 gives the change in D with increasing ϕ_H as a function of PEO molecular weight for bulk samples and thin films. D for bulk samples of mixtures with PEO-0.6 showed a slight *decrease* in D at a low fraction. For mixtures with PEO-1.5, D does not increase at low ϕ_H but then increase gradually at higher ϕ_H. Once the M_w of PEO is greater than 6000, D increased linearly with ϕ_H for PEO but was independent of the M_w of PEO homopolymer. This indicates that the degree of the localization of PEO chains within the cylindrical microdomains is the same regardless of the PEO molecular weight, once the PEO molecular weight is greater than a critical molecular weight. Furthermore, D is very similar to that for bulk samples with higher molecular weights of PMMA (60 000 and 127 000) at a given ϕ_H as shown in Figure 6a. From the results in Figures 6 and 8, it can be concluded that, at a given homopolymer molecular weight, PEO chains are more localized inside the cylindrical microdomains than PMMA homopolymers.

The change of D/D_0 for thin films with PEO as a function of ϕ_H for different PEO molecular weights is shown as Figure 8b. Mixtures with PEO-18 and PEO-105 behave similarly. D/D_0 increased very sharply at low volume fractions of PEO and then more slowly as the volume fraction was increased further. Also, D/D_0 in thin film is greater than that in bulk sample at a given volume fraction of PEO.

IV. Discussion

The degree of localization of the homopolymer within cylindrical PMMA microdomains can be estimated. For cylindrical microdomains, D can be written as

$$D = \frac{R}{\sqrt{(2/\sqrt{3}\pi)f}} \tag{1}$$

where f is the volume fraction of the minor phase (namely, PMMA block plus a homopolymer in a mixture) and R is the radius of the minor phase. D_0 for neat PS−PMMA is obtained from eq 1 in the absence of added homopolymer with microdomains of radius R_0 and volume fraction f_0 (0.3). From eq 1, the change in D with ϕ_H is given by

$$\frac{D}{D_0} = \left(\frac{R}{R_0}\right)\sqrt{\frac{f_0}{f}} \tag{2}$$

$$\frac{f_0}{f} = 1 - \phi_H(1 - f_0) \tag{3}$$

where ϕ_H is the homopolymer volume fraction in the minor phase.

However, the dependence of R/R_0 on ϕ_H should be known to obtain D/D_0 at a given ϕ_H. First, the volume of PS matrix (V_{matrix}) in a repeat unit of the hexagonally packed cylinders with length h is proportional to the number of block copolymer chains (n_{block}) in the same unit. The interfacial area (A_i) between A and B block is the product of the areal density (Σ in nm^2/chain) and n_{block} in the same unit.

$$A_i = \Sigma n_{block} \tag{4}$$

$$\frac{V_{matrix}}{V_{matrix,0}} = \frac{n_{block}}{n_{block,0}} \tag{5}$$

Here, the subscript "0" represents neat block copolymer. Since the volume of one cylindrical domain (V_{cyl}) is given by $V_{matrix}\,[f/(1-f)]$, we have

$$\frac{V_{cyl}}{A_i} = \frac{\pi R^2 h}{2\pi R h} = \frac{R}{2} = \left(\frac{V_{matrix,0}}{n_{block,0}}\right)\left(\frac{f}{1-f}\right)\left(\frac{1}{\Sigma}\right) \tag{6}$$

Equation 6 gives the ratio of R/R_0:

$$\frac{R}{R_0} = \left(\frac{1-f_0}{f_0}\right)\left(\frac{f}{1-f}\right)\left(\frac{\Sigma_0}{\Sigma}\right) = \left(\frac{\Sigma_0}{\Sigma}\right)/(1-\phi_H) \tag{7}$$

From eqs 2 and 7, we have

$$\frac{D}{D_0} = \left(\frac{1-f_0}{1-f}\right)\sqrt{\frac{f}{f_0}}\left(\frac{\Sigma_0}{\Sigma}\right) = \left(\frac{\sqrt{1-\phi_H(1-f_0)}}{1-\phi_H}\right)\left(\frac{\Sigma_0}{\Sigma}\right) \tag{8}$$

Thus, to obtain the dependence of D/D_0 on ϕ_H, we should know the dependence of Σ/Σ_0 on ϕ_H. This can be obtained from the minimization of the free energy. Here, we consider a core−shell shape for the cylindrical microdomain consisting of corona (PS block chain; region I) and core (PMMA block chain + homopolymer; regions II and III) as schematically shown in Figure 10. Also, it is assumed that for the simple estimation the concentration profile of a homopolymer at the interface between regions II and III is given by a step function, although an actual concentration profile might be a hyperbolic tangent[41] or a Gaussian.[13,30] Namely, region III with a radius of l_{local} contains the homopolymer only. Region II with a half-thickness of l_{mix} consists of PMMA block chains and the homopolymer chains. The concentration profiles of the homopolymer in region II is uniform. Region I with a half thickness of l_{matrix} contains only PS block chains.

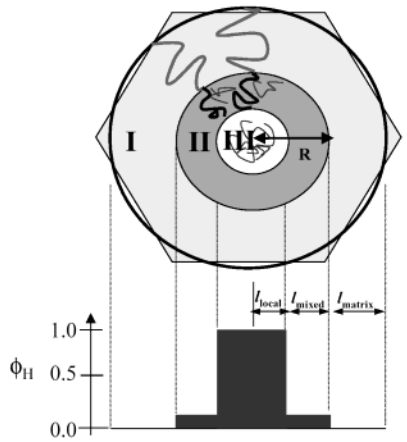

Figure 9. A schematic for a homopolymer distribution within cylindrical microdomains. The *y*-axis is the homopolymer concentration: region I with PS block chain only, region II where the homopolymer chains are uniformly distributed, and region III containing the homopolymer only.

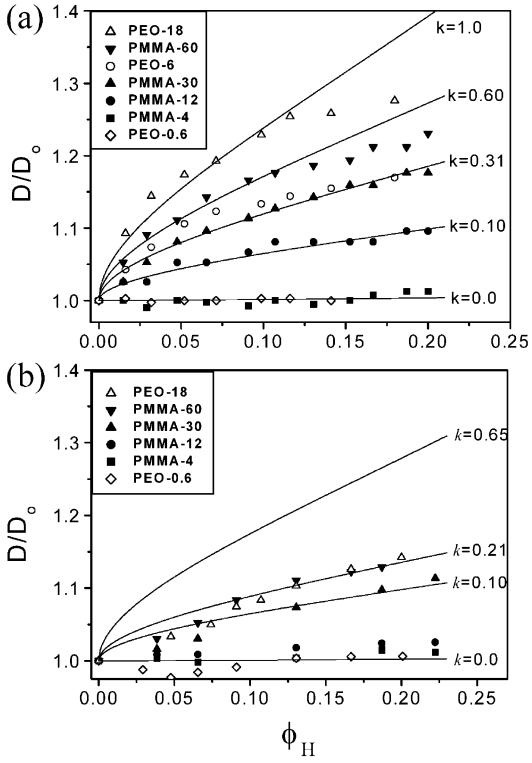

Figure 10. Increase in D with ϕ_H in thin film (a) and in bulk (b): symbols are experimental results, and curves are predictions with the adjustable parameter of k.

We introduce one adjustable parameter k, the volume fraction of the homopolymer localized to the center of cylindrical microdomains (region III). In this situation, we have

$$\frac{l_{local}^2}{R^2} = k\phi_H \tag{9}$$

$$l_{mix} = R(1 - \sqrt{k\phi_H}) \tag{10}$$

A perfect localization of a homopolymer corresponds to $k = 1$, whereas uniform solubilization of a homopolymer

inside cylindrical microdomains is expected for $k = 0$. On the other hand, l_{matrix} is given by

$$l_{matrix} = R\,\frac{1-\sqrt{f}}{\sqrt{f}} \tag{11}$$

The free energy per chain, F_{chain}, for a binary mixture of A−B block copolymer and B homopolymer, whose concentration distribution is described by Figure 9, is expressed by [26,42]

$$\frac{F_{chain}}{k_BT} = \frac{\gamma_0}{k_BT}\Sigma + \frac{1}{2}(\alpha_A^{\,2} + \alpha_B^{\,2} + 2/\alpha_A + 2/\alpha_B - 6) + \frac{N_B}{2}\left(\frac{1-\phi_H}{N_B}\ln(1-\phi_H) + \frac{\phi_H}{P_B}\ln\phi_H\right) \tag{12}$$

$$\alpha_A = \frac{l_{matrix}}{\sqrt{N_A}b};\quad \alpha_B = \frac{l_{mix}}{\sqrt{N_B}b} \tag{13}$$

Here, k_B is the Boltzmann constant, T is the absolute temperature, γ_0 is the interfacial tension, N_A (and N_B) is the degree of polymerization of block A (and B), P_B is the degree of polymerization of homopolymer B, and b is the Kuhn length.

Since l_{matrix} and l_{mix} can be expressed by Σ, we have the equilibrium value of Σ (Σ_{min}) from $(\partial F_{chain}/\partial\Sigma)_{\Sigma_{min}} = 0$ (see Appendix).

$$\Sigma_{min} = \left[\frac{4\sqrt{6}N^{3/2}b^6(B_A^{\,2} + B_B^{\,2})}{\sqrt{\chi N} + (\sqrt{6}/2)(B_A^{\,-1} + B_B^{\,-1})}\right]^{1/3} \tag{14}$$

Here, B_A and B_B are given by

$$B_A \equiv \frac{\sqrt{1-f_0}}{(1+\sqrt{f})/\sqrt{f}},\quad B_B \equiv \frac{\sqrt{f_0}}{(1-\phi_H)/(1-\sqrt{k\phi_H})} \tag{15}$$

and N is the total degree of polymerization ($N = N_A/(1-f_0) = N_B/f_0$). Since $\Sigma_{0,min}$ for a neat block copolymer is obtained from eq 14 with $\phi_H = 0$ and $f = f_0$, we have $\Sigma_{min}/\Sigma_{0,min}$.

$$\frac{\Sigma_{min}}{\Sigma_{0,min}} = \left(\frac{\sqrt{\chi N} + (\sqrt{6}/2)(B_{A,0}^{\,-1} + B_{B,0}^{\,-1})}{\sqrt{\chi N} + (\sqrt{6}/2)(B_A^{\,-1} + B_B^{\,-1})}\right)^{1/3}\left(\frac{B_A^{\,2} + B_B^{\,2}}{B_{A,0}^{\,2} + B_{B,0}^{\,2}}\right)^{1/3} \tag{16}$$

in which $B_{A,0}$ and $B_{B,0}$ are obtained from eq 15 by setting $f = f_0$ and $\phi_H = 0$. For $\chi_{PS/PMMA} \sim 0.028$ and $N \sim 800$, we found that the first term in eq 16 is close to unity regardless of k values for $\phi_H < 0.2$.

Figure 10 gives calculated and measured D/D_0 for both thin film and bulk on the basis of eqs 8 and 16 with only one adjustable parameter k for various mixtures with different molecular weights of PMMA and PEO homopolymers. In both the thin film (a) and bulk (b) cases, k increased with increasing molecular weight of the homopolymer. However, k values for the thin films are much larger than those in the bulk at a given homopolymer molecular weight. For instance, k in thin films for mixtures with PEO-18 was ~1.0, but 0.21 in the bulk. This indicates that PEO-18 chains in the thin film are highly localized to the center of PMMA cylindrical microdomains with very limited interpenetration into the PMMA block chains. In the bulk, using this argument, only 21% of PEO-18 chains are localized to the center of the cylindrical microdomains.

It is also seen in Figure 10 that, at a given molecular weight, k for mixtures with PEO is greater than that for mixtures with PMMA, indicating that PEO chains are more localized to the center of cylindrical microdomains. This can be explained by the degree of localization of the homopolymer within cylindrical microdomains that depends on χ between the homopolymer and PMMA block and that between the homopolymer and PS block. Since $\chi_{PEO/PS} > \chi_{PMMA/PS}$, PEO will minimize contact with the PS block. Thus, PEO chains are likely to locate far from the PS−PMMA interface.

Finally, we consider why the increase of D/D_0 with ϕ_H in thin films is larger than in bulk samples at a given homopolymer molecular weight. One reason may be the difference of the degree of segregation in block copolymer in thin film and bulk. For neat PS−PMMA, D_0 in thin film was 35.5 nm, which is larger than that (34.1 nm) in the bulk. This suggests that in thin films the PMMA chains are more stretched at the interface between the microdomains than those in bulk samples because of strong confinement of block chains to the substrate.

V. Conclusions

The miscibility between PMMA homopolymer and PMMA block in thin films was enhanced compared with that in bulk samples. At a given molecular weight of homopolymer, the increase of D in thin films was larger than that in bulk samples, which indicates more localization of the homopolymer to the center of the cylindrical microdomains in thin films. The increase of D was rapid at low volume fractions of PMMA homopolymer but slowed as the PMMA concentration increased. The increase of D for mixtures with high molecular weights becomes saturated above a certain molecular weight.

For mixtures with PEO homopolymer, the behavior of D was the same as mixtures with PMMA homopolymer, except that the saturation of D was reached at much smaller molecular weight than mixtures with PMMA homopolymer. From a model analysis, PEO chains in thin films with molecular weight higher than 18 000 appear to be completely localized to the center of cylindrical microdomains, whereas in bulk the localization is diminished. Thus, complete localization to the center of the microdomains was possible in thin films with PEO, but not with PMMA homopolymer. This is attributed to the strong repulsive interaction between PEO and PS.

Acknowledgment. This work was supported by National RND project for nano science and technology, the Korea Research Foundation (KRF-2002-05-D00008), National Research Laboratory by MOST, the Department of Energy, Office of Basic Energy Sciences under contract DE-FG02-96ER45612, National Science Foundation under the Partnership in Nanotechnology (CTR-9871782), and the Material Research Science and Engineering Center at the University of Massachusetts. Small-angle X-ray scattering was performed at PLS beamline supported by POSCO and KOSEF.

Appendix. Derivation of Eq 14

First, we calculate the volume of one chain of PMMA block (block B)

$$N_B b^3 = \frac{V_{mix} - V_{homo(II)}}{n_{block}} = \frac{V_{mix}}{n_{block}}\left(\frac{1-\phi_H}{1-k\phi_H}\right) \quad \text{(A1)}$$

in which V_{mix} and $V_{homo(II)}$ are the total volume of the region II and the volume occupying the homopolymer located at region II and given by $\pi R^2 h(1 - k\phi_H)$ and $\pi R^2 h(\phi_H - k\phi_H)$, respectively. h is the length of one cylinder. Also, V_{mix} and the interfacial area (A_i) can be given by

$$\frac{V_{mix}}{A_i} = \frac{V_{cyl}(1-k\phi_H)}{2\pi R h} = \frac{R(1-k\phi_H)}{2} \quad \text{(A2)}$$

Since the area per a block copolymer chain (Σ) is simply given by A_i/n_{block}, we have

$$N_B b^3 = \frac{R}{2}(1-k\phi_H)\left(\frac{1-\phi_H}{1-k\phi_H}\right)\Sigma = \frac{l_{mix}}{2}\left(\frac{1-\phi_H}{1-\sqrt{k\phi_H}}\right)\Sigma \quad \text{(A3)}$$

Here, eq 10 is used.

The volume of one chain of PS block (block A) is similarly calculated as follows:

$$N_A b^3 = \frac{V_{matrix}}{n_{block}} \quad \text{(A4)}$$

Similarly, the volume of PS matrix (V_{matrix}) and A_i is given by

$$\frac{V_{matrix}}{A_i} = \frac{V_{cyl}[(1-f)/f]}{2\pi R h} = \frac{R}{2}\left(\frac{1-f}{f}\right) \quad \text{(A5)}$$

Substitution of eq A5 and $\Sigma = A_i/n_{block}$ into eq A4 becomes

$$N_A b^3 = \frac{R}{2}\left(\frac{1-f}{f}\right)\Sigma = \frac{l_{matrix}}{2}\left(\frac{1+\sqrt{f}}{\sqrt{f}}\right)\Sigma \quad \text{(A6)}$$

Here, eq 11 was used. From eqs A3, A6, and 12 with the aid of $\gamma_0/k_B T = (\chi/6)^{1/2}/b^2$,[41] we have

$$\frac{F_{chain}}{k_B T} = \left[\frac{1}{\sqrt{N}b^2}\left(\sqrt{\frac{\chi N}{6}} + \frac{1}{2}(B_A^{-1} + B_B^{-1})\right)\right]\Sigma + 2Nb^4(B_A^2 + B_B^2)\Sigma^{-2} + C \quad \text{(A7)}$$

B_A and B_B are given in eq 15, and C is the entropy of the mixing contribution to free energy (the last term in eq 12) which does not depend on Σ, l_{mix}, and l_{matrix}. From $(\partial F_{chain}/\partial\Sigma)_{\Sigma_{min}} = 0$, Σ_{min} is obtained and given in eq 14. Note that Tanaka et al.[10] derived an equation to predict the change of the lattice domain with ϕ_H for a uniform distribution of the homopolymer in mixtures of a block copolymer having lamellae microdomains and a homopolymer. However, the term of $2/\alpha_A + 2/\alpha_B$ in eq 12 was neglected.[10]

Figure 11 shows the change of $(l/l_0)_{matrix}$, $(l/l_0)_{mix}$, $[(l/l_0)_{matrix} + (l/l_0)_{mix}]/2$, R/R_0, and D/D_0 with increasing ϕ_H at two values of k (1.0 and 0). From the results of the decrease of $(l/l_0)_{mix}$ with ϕ_H as shown in Figure 11a, l_{mix} of region II cannot be the same as R_0 of neat block copolymer even when the homopolymer chains are completely localized within the center of the cylindrical microdomains. Namely, $R_{local} \neq R_0 + R_{H,local}$. Here, R_{local} and $R_{H,local}$ are the total radii of cylindrical microdomains, including the homopolymer and homopolymer itself, respectively, for a complete localization.

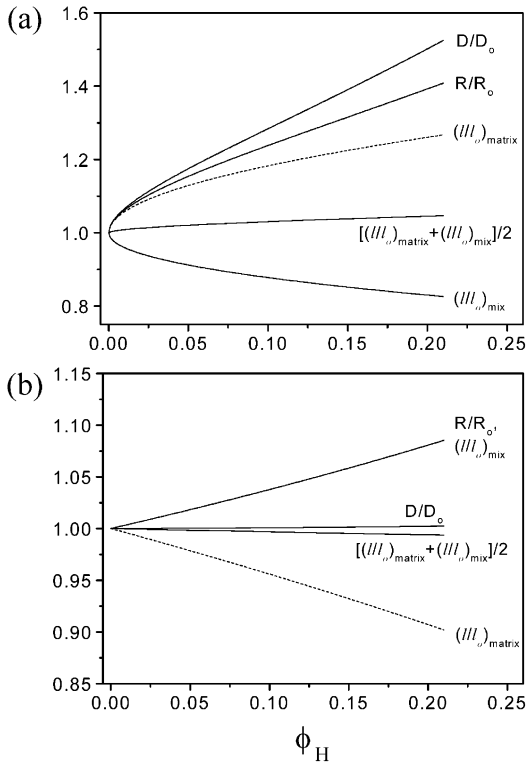

Figure 11. Change of R/R_0, D/D_0, $(l/l_0)_{mix}$, $(l/l_0)_{matrix}$, and $[(l/l_0)_{matrix} + (l/l_0)_{mix}]/2$ with ϕ_H at two values of k: (a) $k = 1$ and (b) $k = 0$. Here, the subscript "0" represents neat PS−PMMA itself.

For a mixture consisting of a block copolymer with a homopolymer whose microdomain morphology is lamellar and the homopolymer localized completely within the lamellar microdomain, $L_L = L_{H,L} + L_0$. Here, L_L, $L_{H,L}$, and L_0 are the lamellar thickness for lamellar microdomain consisting of the homopolymer, homopolymer itself, and one block in the neat block copolymer, respectively. In this case, D/D_0 (in which D and D_0 are the lamellar domain spacing for a mixtures with the homopolymer and neat block copolymer itself, respectively) is given by[10,32,33]

$$\left(\frac{D}{D_0}\right)_{LAM} = \left(\frac{1-\phi_H(1-f_0)}{1-\phi_H}\right)\left(\frac{\Sigma_0}{\Sigma}\right) = \left(\frac{1}{1-\Phi_H}\right)\left(\frac{\Sigma_0}{\Sigma}\right) \quad \text{(A8)}$$

in which Φ_H is the volume fraction of the homopolymer in the total mixture and smaller than ϕ_H because $\Phi_H = \phi_H f_0/[1 - \phi_H(1 - f_0)]$.

Since Σ (or areal density) at the interface of the block copolymer is constant regardless of ϕ_H due to the complete localization of the homopolymer,[10] $(D/D_0)_{LAM}$ does not increase with ϕ_H compared with D/D_0 for cylindrical microdomains. For instance, $(D/D_0)_{LAM}$ at $\phi_H = 0.2$ is 1.075 for $f_0 = 0.3$ and 1.125 for $f_0 = 0.5$, which is much smaller than that (1.39) for cylindrical microdomains shown in Figure 11a. A small increase in D for lamellar microdomains at lower values of ϕ_H was reported.[10,13,32,33]

The large increase in D/D_0 with ϕ_H for a block copolymer having cylindrical microdomain is due to curvature of cylindrical microdomains. When eq A8 is compared with eq 8 along with eq 16, the two different expressions between cylindrical microdomains and lamel-

lar microdomains exist: (1) The first term, namely, $\sqrt{1-\phi_H(1-f_0)}/(1-\phi_H)$ vs $[1-\phi_H(1-f_0)]/(1-\phi_H)$, becomes 1.15 and 1.075, respectively, at $\phi_H = 0.2$. (2) The second term, $\Sigma_{min}/\Sigma_{0,min}$, decreases steadily with ϕ_H for cylindrical microdomains, whereas it does not change with ϕ_H for lamellar microdomains. For $k = 1$, this becomes 0.832 at $\phi_H = 0.2$. (Thus, the contribution of $\Sigma_{0,min}/\Sigma_{min}$ to D/D_0 becomes 1.20.)

It is also seen in Figure 11 that, with increasing ϕ_H, $(l/l_0)_{matrix}$ increases for $k = 1$ but it decreases for $k = 0$, although the change is smaller than that of R in both cases. Finally, the value of $[(l/l_0)_{matrix} + (l/l_0)_{mix}]/2$ is not far from unity regardless of ϕ_H, which suggests that the increase and decrease of these two factors are compensated by each other.

References and Notes

(1) Mansky, P.; Harrison, C. K.; Chaikin, P. M.; Register, R. A.; Yao, N. *Appl. Phys. Lett.* **1996**, *68*, 2586.
(2) Park, M.; Harrison, C. K.; Chaikin, M.; Register, R. A.; Adamson, D. H. *Science* **1997**, *276*, 1407.
(3) Averopoulos, A.; Chan, V. Z.-H.; Lee, V. Y.; No, D.; Miller, R. D.; Hadjichristidis, N.; Thomas, N. L. *Chem. Mater.* **1998**, *10*, 2109.
(4) Thurn-Albrecht, T.; Schotter, J.; Kästle, A.; Emley, N.; Shibauchi, T.; Krusin-Elbaum, L.; Guarini, K.; Black, C. T.; Tuominen, M. T.; Russell, T. P. *Science* **2000**, *290*, 2126.
(5) Thurn-Albrecht, T.; Steiner, R.; DeRouchey, J.; Stafford, C. M.; Huang, E.; Ball, M.; Tuominen, M.; Hawker, C. J.; Russell, T. P. *Adv. Mater.* **2000**, *12*, 787.
(6) Black, C. T.; Guarini, K. W.; Milkove, K. R.; Baker, S. M.; Tuominen, M. T.; Russell, T. P. *Appl. Phys. Lett.* **2001**, *79*, 409.
(7) Bates, F. S.; Fredrickson, G. H. *Annu. Rev. Phys. Chem.* **1990**, *41*, 525.
(8) Hamley, I. W. *The Physics of Block Copolymers*; Oxford University Press: Oxford, 1998.
(9) Hashimoto, T.; Tanaka, H.; Hasegawa, H. *Macromolecules* **1990**, *23*, 4378.
(10) Tanaka, H.; Hasegawa, H.; Hashimoto, T. *Macromolecules* **1991**, *24*, 240.
(11) Hashimoto, T.; Izumitani, T.; Ono, K. *Macromol. Symp.* **1995**, *98*, 925.
(12) Hasegawa, H.; Hashimoto, T. Self-assembly and morphology of block copolymer systems. In *Comprehensive Polymer Science. Suppl. 2*; Aggarwal, S. L., Russo, S., Eds.; Pergamon: London, 1996; p 497.
(13) Winey, K. I.; Thomas, E. L.; Fetters, L. J. *Macromolecules* **1991**, *24*, 6182.
(14) Lowenhaupt, B.; Steurer, A.; Hellmann, G. P.; Gallot, Y. *Macromolecules* **1994**, *27*, 908.
(15) Frielinghaus, H.; Almdal, K.; Mortensen, K. *Macromol. Symp.* **2000**, *149*, 63.
(16) Balsara, N. P.; Jonnalagadda, S. V.; Lin, C. C.; Han, C. C.; Krishnamoorti, R. *J. Chem. Phys.* **1993**, *99*, 10011.
(17) Maurer, W. W.; Bates, F. S.; Lodge, T. P.; Almdal, K.; Mortensen, K.; Fredrickson, G. H. *J. Chem. Phys.* **1998**, *108*, 2989.
(18) Nojima, S.; Roe, R. J. *Macromolecules* **1987**, *20*, 1866.
(19) Jeon, K. J.; Roe, R. J. *Macromolecules* **1994**, *27*, 2439.
(20) Lee, S. H.; Koberstein, J. T.; Quan, X.; Gancarz, I.; Wingnall, G. D.; Wilson, F. C. *Macromolecules* **1994**, *27*, 3199.
(21) Baek, D. M.; Han, C. D.; Kim, J. K. *Polymer* **1992**, *33*, 4821.
(22) Kimishma, K.; Hashimoto, T.; Han, C. D. *Macromolecules* **1995**, *28*, 3842.
(23) Vaidya, N. Y.; Han, C. D. *Polymer* **2002**, *43*, 3047.
(24) Hamdoun, B.; Ausserre, D.; Cabull, V.; Joly, S. *J. Phys. II* **1996**, *6*, 503.
(25) Floudas, G.; Hadjichristidis, N.; Stamn, M.; Likhtman, A. E.; Semenov, A. N. *J. Chem. Phys.* **1997**, *106*, 3318.
(26) Noolandi, J.; Hong, K. M. *Macromolecules* **1982**, *15*, 482.
(27) Whitemore, M. D.; Noolandi, J. *Macromolecules* **1985**, *18*, 657.
(28) Semenov, A. N. *Macromolecules* **1993**, *26*, 2273.
(29) Matsen, M. W. *Macromolecules* **1995**, *28*, 5765.
(30) Mayes, A. M.; Russell, T. P.; Satija, S. K.; Majkrzak, C. F. *Macromolecules* **1992**, *25*, 6523.
(31) Matsushita, Y.; Torikai, N.; Mogi, Y.; Noda, I.; Han. C. C. *Macromolecules* **1993**, *26*, 5698.
(32) Torikai, N.; Takabyashi, N.; Noda, I.; Koizumi, S.; Morii, Y.; Matsushita, Y. *Macromolecules* **1997**, *30*, 5698.
(33) Orso, K. A.; Green, P. F. *Macromolecules* **1999**, *32*, 1087.
(34) Smith, M. D.; Green, P. F.; Saunders, R. *Macromolecules* **1999**, *32*, 8392.
(35) Huang, E.; Rockford, L.; Russell, T. P.; Hawker, C. J. *Nature (London)* **1998**, *395*, 757. Huang, E.; Russell, T. P.; Harrison, C.; Chaikin, P. M.; Register, R. A.; Hawker, C. J.; Mayes, J. *Macromolecules* **1998**, *31*, 7641.
(36) Bolze, J.; Kim, J.; Huang, J.; Rah, S.; Youn, H. S.; Lee, B.; Shin, T. J.; Ree, M. *Macromol. Res.* **2002**, *10*, 2.
(37) Xu; T.; Kim, H. C.; Derouchey, J.; Seney, C.; Levesque, C.; Martin, P.; Stafford, C. M.; Russell, T. P. *Polymer* **2001**, *42*, 9091.
(38) Jeong, U.; Kim, H. C.; Rodriguez, R. L.; Tsai, I. Y.; Stafford, C. M.; Kim, J. K.; Hawker, C. J.; Russell, T. P. *Adv. Mater.* **2002**, *14*, 274.
(39) Frielinghaus, H.; Mortensen, K.; Almdal, K. *Macromol. Symp.* **2000**, *149*, 63.
(40) Shearmur, T. E.; Clough, A. S.; Drew, D. W.; van der Grinten, M. G. D.; Jones, R. A. L. *Macromolcules* **1996**, *29*, 7269.
(41) Helfand, E. Tagami, Y. *J. Chem. Phys.* **1972**, *56*, 3592.
(42) The second term in eq 12 was obtained from an elongational mode mode. For a shear mode, this term becomes $(\alpha_A^2 + \alpha_B^2 + 1/\alpha_A^2 + 1/\alpha_B^2 - 4)/2$ instead of $(\alpha_A^2 + \alpha_B^2 + 2/\alpha_A + 2/\alpha_B - 6)/2$. However, even when the expression for a shear mode is used, the change of $\Sigma_{min}/\Sigma_{0,min}$ with ϕ_H is almost the same as that predicted by eq 16.

MA034179K